Bioelectrochemistry 154 (2023) 108510

Contents lists available at ScienceDirect

Bioelectrochemistry

journal homepage: www.journals.elsevier.com/bioelectrochemistry

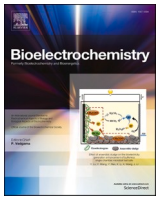

# Tumor location on electroporation therapies by means of multi-electrode structures and machine learning

P. Briz *, B. López-Alonso, H. Sarnago, J.M. Burdío, O. Lucía

*Department of Electronic Engineering and Communications, I3A. University of Zaragoza, Maria de Luna 1, Zaragoza 50018, Spain*

ARTICLE INFO

*Keywords:*
Electroporation
Pulsed electric field
Machine learning
Tumor ablation

ABSTRACT

Electroporation is a phenomenon produced in the cell membrane when it is exposed to high pulsed electric fields that increases its permeability. Among other application fields, this phenomenon can be exploited in a clinical environment for tumor ablation therapies. In this context to achieve optimum results, it is convenient to focus the treatment on the tumor tissue to minimize side effects. In this work, a pre-treatment tumor location method is developed, with the purpose of being able to precisely target the therapy. This is done by taking different impedance measurements with a multi-output electroporation generator in conjunction with a multi-electrode structure. Data are processed by means of a vector of independent artificial neural networks, trained and tested with simulation data, and validated with phantom gels. This algorithm proved to provide suitable accuracy in spite of the low electrode count compared to the number of electrodes of a standard electrical impedance tomography device.

## 1. Introduction

Electroporation phenomenon consists of cell membrane permeabilization when they are exposed to high intensity pulsed electric fields. It has many application areas, such as food processing, biotechnology or medicine [1–8]. In this last-mentioned field, one of the most important clinical applications is tumor ablation.

Electroporation based treatments for tumor ablation do not present the inconveniences of thermal based procedures, such as microwave or radiofrequency ablation, so their popularity is rising in the latest years [9–11]. Due to their non-thermal character, they can be used for treating highly irrigated tissues. They also preserve the connective matrix of the blood vessels [12], so they allow to minimize side effects on healthy tissue irrigated by blood vessels passing through or near ablated areas. In this way, faster recovery times after surgery are achieved [13]. However, there are still challenges to overcome, one of them being to concentrate the treatment on the tumor area where this paper is focused on.

Because tumor tissue conductivity is higher than surrounding healthy tissue conductivity, it can be difficult to target the treatment into the tumor, as a consequence of the electric field concentrating on the less conductive tissue. Nowadays, clinical electroporation treatments tend to increase the electric field intensity or the number of pulses in order to ensure proper ablation of the desired area. This can cause side effects such as thermal damage [14,15], and unnecessarily ablating healthy tissue. Sometimes, it may even be really challenging to ensure that there is enough electric field on the tumor to treat it. On this way, a pre-treatment method to locate tumor tissue between parallel plate-based electrodes, with the system used to apply the treatment, is proposed. It is based on different directions impedance measurements, processed by a machine learning algorithm, that outputs the location of tumor tissue between electrodes, without external equipment, in order to target the treatment on tumor tissue in real time.

Existing methods to locate tumor tissue before treatment are mainly based on MRI or echography, but they cannot be used while plate electrodes are placed, so it is not possible to observe the position of the tumor in relation to the electrodes. The method developed in this work is based on the same principle of an electrical impedance tomography (EIT), where impedance is measured on different parts of the tissue. Currently, several EIT based methods exist to monitor treatments [16–18], but not for locating tumor tissue, and they also require disconnecting the measurement system to avoid damaging it with high voltage electroporation pulses. The main difference between the proposed method and an EIT is that while EIT can be used for mapping the impedance of the tissue and therefore finding the most conductive areas, it does not directly output the areas with tumor tissue. Moreover, the

* Corresponding author.
*E-mail address:* pbriz@unizar.es (P. Briz).

https://doi.org/10.1016/j.bioelechem.2023.108510
Received 31 January 2023; Received in revised form 2 June 2023; Accepted 12 July 2023
Available online 22 July 2023

purposed method does not try to reproduce an impedance map of the tissue between the electrodes, but it detects areas with tumor tissue where the treatment must be focused on in order to maximize the effectiveness of the treatment, while also minimizing side effects on the surrounding healthy tissue. Besides, traditional EIT algorithms require a high electrode count and an increased number of measurements to achieve a useful precision [19]. This last situation is where machine learning algorithms can overcome the difficulties of traditional EIT algorithms, and therefore, they are selected in this work. A preliminary proposal of this studio was presented [20] on the 4th World Congress on Electroporation.

Machine learning algorithms, while still having some drawbacks, are becoming increasingly popular in many application fields. As an example, there are high frequency irreversible electroporation treatment planning methods that make use of neural networks [21].

## 2. Material and methods

This section presents the measurement system that enabled the collection of impedance measurements on different parts of the tissue between electrodes. Then, the machine learning algorithm to locate tumor tissue based on the previous measurements is described.

### 2.1. Electroporation and impedance measurement system

In this paper, a versatile multi-output electroporation system has been used for performing the impedance measurements composed by a pair of differential multi-electrodes (Fig. 1 and a multi-output voltage generator [22]. The electrodes used with the inverter are based on two differential parallel plate-based electrodes, but instead single-plate electrodes, they were divided in a 3-by-3 matrix of plates, so each one can be driven independently. This implies voltage can be applied between any combination of plates of an electrode to anyone of the other one, creating electric field vectors with different orientations in different parts of the tissue without relocating the electrodes. In order to apply the desired voltage to each plate of the electrodes, a versatile multi-output inverter specifically designed to be used in conjunction with the mentioned electrodes is necessary in this research. It is not only capable of delivering high voltage pulses (continuously, in bursts, monopolar or bipolar, and so on) but it is also designed to be able to apply low voltage bursts before, during and after the treatment, thus allowing to measure the impedance between electrodes in real time. Thanks to its versatility, it can be employed not only to treat tumor tissue but also to locate tumors before the treatment, which is the main purpose of this paper.

In this research, impedance is obtained at the frequency of 10 kHz. This frequency is chosen because is low enough so that the electrode cables inductance does not add any significant impedance (relative to the tissue) to the measurement, thus providing more precise measurements, while also keeping the measuring time under 100 ms so that energy translated to the tissue ion the measuring process does not heat up the tissue. Also, at frequencies under 100 kHz, impedance difference between tumor and healthy tissue is higher, so it is easier to distinguish between tumor and healthy tissue. In order to calculate impedance, a train of 10 bipolar square pulses, at 10 kHz (1 ms) is applied between the desired electrode plates. Then, the FFT of the measured voltage and current is computed at 10 kHz, and impedance is obtained from those values.

This whole system also enables the application of different high strength electric field vectors on the tumor to increase effectiveness, once tumor tissue locations between the electrodes are known, and monitoring the therapy in real-time, even providing treatment outcome information.

### 2.2. Data processing

The main goal of this research is to find tumors between electrodes, thus allowing to target the electroporation treatment on it.

So as to find tumors, tissue between electrodes is depicted in two layers of 3-by-3 voxels, a total of 18, as shown in Fig. 2b. The objective of this system is to identify the ones containing at least a 5% of tumor tissue, and therefore the tissue regions in which the treatment should be targeted. In order to find tumor tissue, impedance $Z$ between 81 cell combinations is measured by a precision current probe and a 10 kHz train of 10 voltage pulses in each cell combination. The applied electric field is well below the reversible electroporation threshold, so that it does not affect the treatment or communicates any significant energy to the tissue [23,24]. In this work, an amplitude of 20 V is employed in the experimentation procedure. The designed algorithm to process these measurements and find tumor tissue between these electrodes is presented in the next section.

#### 2.2.1. Machine learning algorithm

To process the impedance measurements a machine learning algorithm was developed. It consists of a vector of 18 independent neural networks, $ANN_i$, each one of them with one output $\theta_i$ corresponding to a single voxel (Fig. 3a). Each output $\theta_i$ states if there is ($\theta_i = 1$) or not ($\theta_i = 0$) tumor tissue in the associated voxel shown in Fig. 2b. This vector of neural networks permits them to have less neurons per layer, than a

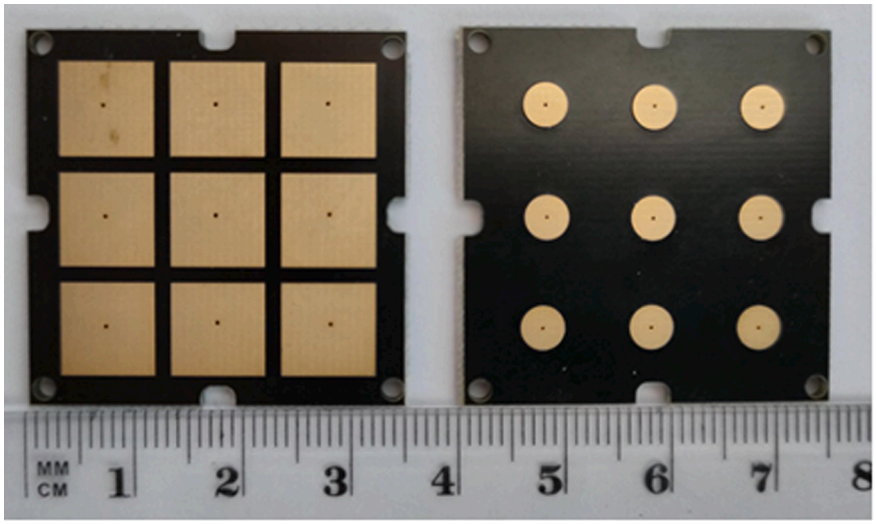


**Fig. 1.** Top and bottom view of the multi-electrodes.

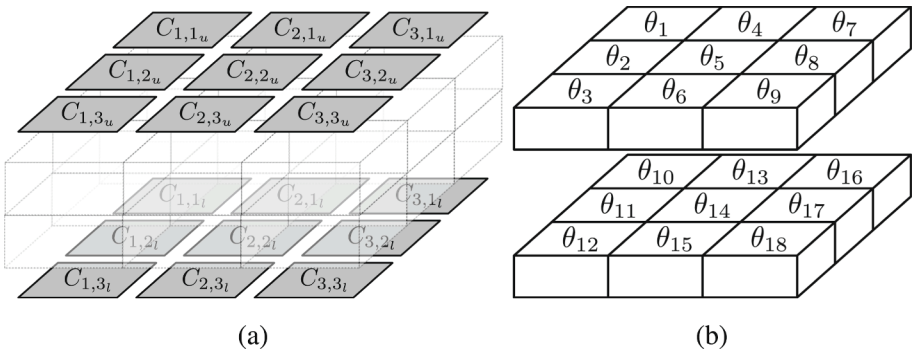


**Fig. 2.** Electrode cells of upper ($C_{j,k_u}$) and lower ($C_{j,k_l}$) electrode with tissue between them (a), and tissue voxels depiction (b), where $\theta_i$ is the output of the neural network corresponding to the voxel.

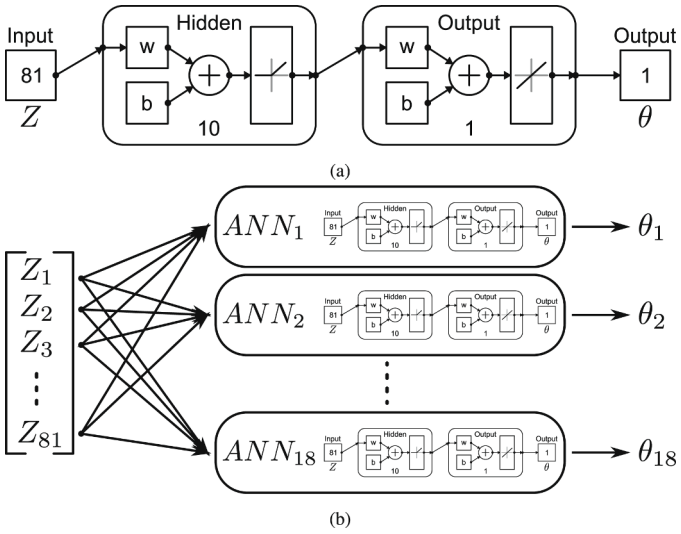


**Fig. 3.** Multi-layered perceptron structure of each independent neural network designed in Matlab® (a). Vector composed of as many independent feedforward neural networks as outputs needed (b). The output $\theta_i$ of each neural network is a true or false statement which describes if the voxel it is associated with contains tumor tissue or not.

more complex network with 18 outputs, which makes them faster and easier to train, with less total parameters to tune, and a smaller training dataset [25,26]. Another advantage of this proposal is its scalability, allowing to solve situations with more voxels. Every neural network is a simple feedforward network, which has a multi-layered perceptron structure, with 10 neurons in a single hidden layer, 81 inputs (the impedance measurements) and 1 output, as shown in Fig. 3a. The implemented transition function is the commonly used ReLU (Rectified Linear Unit, $f(x) = max(0, x)$), because it performs well, is efficient, and allows for a faster training process than other functions. This structure implies that every layer of the network is fully connected in each network, but every neural network is completely independent of the other ones. These neural networks have been trained with a Levenberg-Marquadt algorithm and a cross-validation technique, which is adequate for small neural networks because of its speed of convergence and accuracy [27].

A Levenberg-Marquadt algorithm is a backpropagation algorithm which results in a fast and accurate training method for this problem. Training data is split into 2 main sets: training (85 %) and test (15 %) data. Data split is carried out randomly but ensuring a uniform distribution of cases in the test dataset. This helps performance metrics of neural networks to be realistic.

A big factor in machine learning algorithms is training dataset size: usually the bigger, the better. That said, it depends on several aspects such as training algorithm, validation algorithm, and most importantly total neural network parameters. A common approach is that training partition should be at least 5 to 10 times the number of neural network parameters [26]. In this paper, training dataset size is 7.7 times the total neural network parameters. Total neural network parameters are calculated as follows in (1), where $N_p$ is the total number of parameters, $N_{w_i}$ is the number of weights of each layer, and $N_{b_i}$ is the number of biases of each layer. $N_l$ is the total number of layers, where $i = 0$ represents the input layer (which has no bias parameters), and $l$ the output layer, so that hidden layers go from $i = 1$ to $i = l-1$

$$N_p = \sum_{0}^{l} (N_{w_i} + N_{b_i}). \tag{1}$$

In the proposed neural network architecture, $N_w = 830$ and $N_b = 12$, so $N_p = 842$.

Another consideration to improve network performance and avoid parameters overfitting, is to implement a cross-validation technique in the training process. Training data is cross folded in 5 sets; 20 % of the training set is divided into a validation subset. This validation set is needed to calculate the error of the network with the current training state, and when it starts to increase, even if the error of the training set continues to decrease, the training process stops, to avoid overtraining. This iterative process is repeated 5 times (as many as cross-folding sets), each with a fold of the training set, to achieve the optimal network parameters. Cross-validation technique maximizes training data while also providing validation accuracies to the training algorithm, which is important in this situation where training partition size is smaller than 10 times the total number of parameters to tune. Finally, each network error is tested with the test partition to calculate the accuracy of the networks with new data. Test partition is completely new for the neural networks after training.

### 2.2.2. *Finite element model*

In order to train the machine learning algorithm, a finite element model has been developed by means of the software COMSOL Multiphysics® and Matlab®, using the Electric Currents interface provided by COMSOL® provides. It considers the electric properties of tissues to determine the electric field distribution. Fig. 4 shows the geometry of the model. The model is based on a block that represents the biological tissue between the electrodes, and then the multi-electrodes. The multi-electrodes are modeled using the built-in materials of COMSOL®, i.e. copper and FR4. Then, the block that represents the biological tissue is composed by a $15 \times 15 \times 6$ cell structure. Every cell has the same dimensions, and in the COMSOL® model each one is an independent entity. In order to represent tumor masses and healthy tissue heterogeneity, it is modeled using three different materials: two of them are used for modeling healthy tissue and the third one for modeling

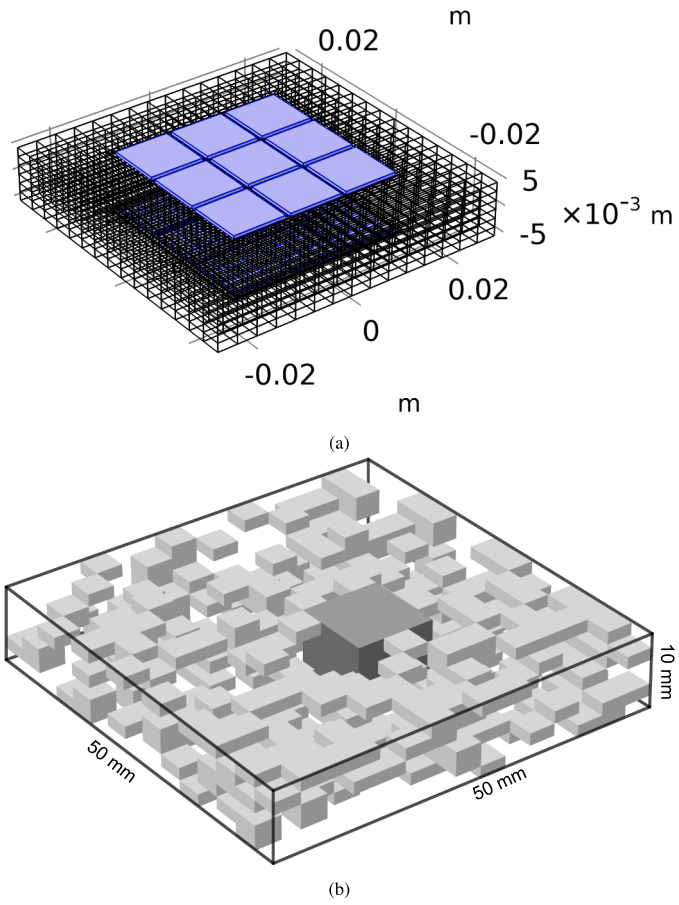


**Fig. 4.** (a) COMSOL® generic model without biological tissue material assignment, where electrode plates are depicted in blue, and the entities representing biological tissue can be seen like a coarse mesh. (b), COMSOL® model with material distribution; tumor tissue in dark gray, base tissue 1 in light gray and base tissue 2 is invisible in this representation to better show the material distribution. Every case has a different distribution of materials 1 and 2, and a different tumor size and position.

tumor tissue. Materials are assigned to the corresponding cells through MATLAB® in every simulation.

To assign the tumor material, firstly tumor center is located randomly in the block, attending tumor size, and ensuring that, if there is more than one tumor, they are not touching each other. Then, depending on tumor size, tumor material is also assigned to the corresponding adjacent cells. After selecting the cells depicting the tumor mass, two materials are assigned to the remaining cells of the entity, following a uniform random distribution so that the average conductivity of the healthy tissue is the average conductivity of the healthy tissue materials. One of the materials has 0.7 times the base conductivity of the healthy tissue and the other one 1.3 times. In this way, healthy tissue heterogeneity is modeled. The parameters assigned to these materials are in Table 1.

In Fig. 4b a picture of the model with materials already assigned is shown. Finally, the base tissue conductivity is determined based on the conductivity range of some biological tissues such as pig liver. Though, it must be noted that impedance measurements are normalized between 0 to 1 in each case before they are used as an input of the neural networks, so that the method works with different tissues without the need for obtaining new simulation data or retraining the networks.

**Table 1**
Main parameters of COMSOL® model.

| Parameter | Value |
|---|---|
| Model dimensions | 50 × 50 × 10 mm |
| Base tissue 1 conductivity | 0.13 S/m |
| Base tissue 2 conductivity | 0.23 S/m |
| Tumor tissue conductivity | 0.36, 0.54, 0.9, 1.8 S/m |
| Min. Tumor size | 3.33 × 3.33 × 1.67 mm |
| Max. Tumor size | 10 × 10 × 8.35 mm |

To improve simulation time, a generic model without tissue materials assigned (but everything else is defined, entities already meshed, and frequency domain study created) is built and saved in an mph file. In the simulation process, this mph file is opened (this is faster than creating the model every time with a MATLAB® function), tissue materials are assigned to the remaining entities, and then 81 simulations are carried out. Each one of these 81 simulations per case changes the ground and electric potential (1 V) boundary conditions, assigning them to their corresponding electrode entities, so that the 81 desired measurements are obtained. A probe that integrates the normal current density is assigned to the same entity that has the ground condition every time, and these results are stored in an array of 81 values for each case.

A total of 7635 models with different tumor sizes and locations have been developed to train and test the neural network. The resulting 81 impedance measurements per case are the inputs of each $ANN_i$ (Fig. 3b, where each $\theta$ is the same as in Fig. 2b).

### 2.3. Experimental evaluation

This section describes an experimental evaluation procedure that can prove the feasibility of the previously exposed method. The experimentation setup shown in Fig. 5 is composed by the following parts:

- Teledyne Lecroy® Wavesurfer 4104HD Digital Oscilloscope with Teledyne Lecroy® HVD3206A high voltage differential probes and Pearson® current sensor model 411.
- Electroporation system: ad hoc high performance multiple output generator with multi-electrodes [22,28].
- Computer with Matlab®, to process and evaluate obtained data.

The above-mentioned oscilloscope, with its voltage probes and current sensors, acquires electrical data from the experiments. Then, data is transferred to computer and it is processed in MATLAB® with the method described before, to obtain the location of “tumor-like”tissue.

In order to validate the designed method described before, samples of phantom gel with known conductivity are used as tissue-mimic materials [29]. Their composition is described in Table 2. Conductivity mostly depends on the sodium chloride concentration, so its concentration establishes the conductivity, between 0.05 S/m and 1.5 S/m. In that way, samples with precise inserts of other samples with higher conductivity are employed to recreate a tumor in a healthy tissue, so that the resulting tumor location estimated by the designed method can be compared with the real location of the “tumor”.

## 3. Results

### 3.1. Neural networks accuracy

Test accuracy of each individual neural network, using simulation test data, is between 99.8 % in the worst cases, corresponding to the voxels of corners, and 100 % on the rest. It is important to know that the total accuracy of the vector of neural networks is the product of all of them, what gives a global test accuracy of 98.95 %. That means the probability to correctly predict every voxel in a case. That said, the errors will be mainly focused on the corners, while the accuracy on the center voxels is still 100 %. Table 3 shows the True Positive rate (TP rate), True Negative rate (TN rate), False Positive rate (FP rate) and False Negative rate (FN rate) of each independent network. It is important to note that validation accuracy and test accuracy are very similar, which is

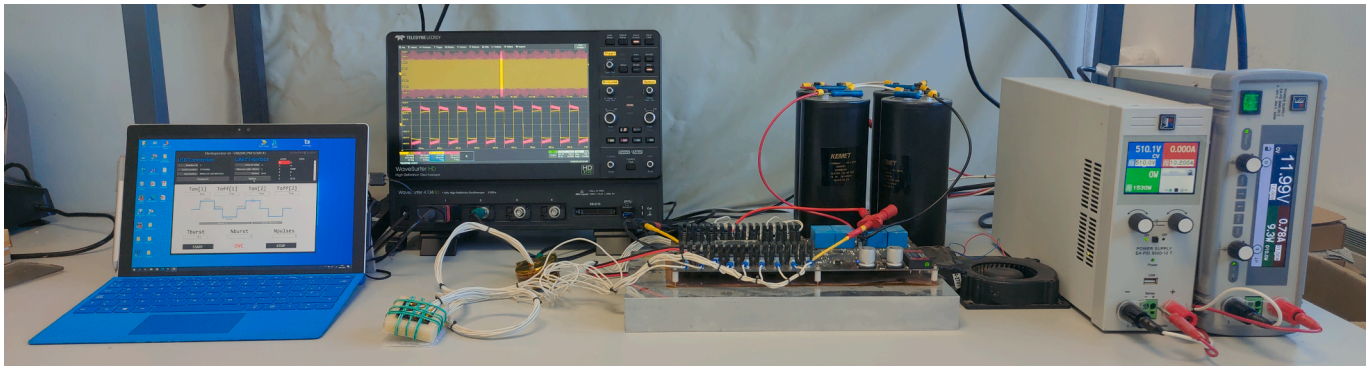

**Fig. 5.** Experimental setup. From left to right: Tablet to control electroporation generator, Oscilloscope (in the back), sample being measured (on front), electroporation voltage generator, High voltage DC source for electroporation, and 12 V dc to supply logic power.

**Table 2**
Tissue-mimic phantom gel composition.

| Ingredient | Quantity (per 70 ml of water) |
|---|---|
| Water | 70 g |
| Glycerin | 2 g |
| Corn flour | 25 g |
| Agar | 1 g |
| Sodium Chloride | from 0.5 g to 2 g |

**Table 3**
Training results of each ANN. True Positive rate (TP rate), True Negative rate (TN rate), False Positive rate (FP rate) and False Negative rate (FN rate) of each network using test data, not used before for training.

| $ANN_i$ | TP rate | TN rate | FP rate | FN rate |
|---|---|---|---|---|
| $ANN_1$ | 0.9986 | 0.9998 | 0.0014 | 0.0002 |
| $ANN_2$ | 1 | 1 | 0 | 0 |
| $ANN_3$ | 0.9986 | 0.9998 | 0.0014 | 0.0002 |
| $ANN_4$ | 1 | 1 | 0 | 0 |
| $ANN_5$ | 1 | 1 | 0 | 0 |
| $ANN_6$ | 1 | 1 | 0 | 0 |
| $ANN_7$ | 0.9987 | 0.9999 | 0.0013 | 0.0001 |
| $ANN_8$ | 1 | 1 | 0 | 0 |
| $ANN_9$ | 0.9991 | 0.9999 | 0.0009 | 0.0001 |
| $ANN_{10}$ | 0.9986 | 0.9998 | 0.0014 | 0.0002 |
| $ANN_{11}$ | 1 | 1 | 0 | 0 |
| $ANN_{12}$ | 0.9986 | 0.9998 | 0.0014 | 0.0002 |
| $ANN_{13}$ | 1 | 1 | 0 | 0 |
| $ANN_{14}$ | 1 | 1 | 0 | 0 |
| $ANN_{15}$ | 1 | 1 | 0 | 0 |
| $ANN_{16}$ | 0.9986 | 0.9998 | 0.0014 | 0.0002 |
| $ANN_{17}$ | 1 | 1 | 0 | 0 |
| $ANN_{18}$ | 1 | 1 | 0 | 0 |

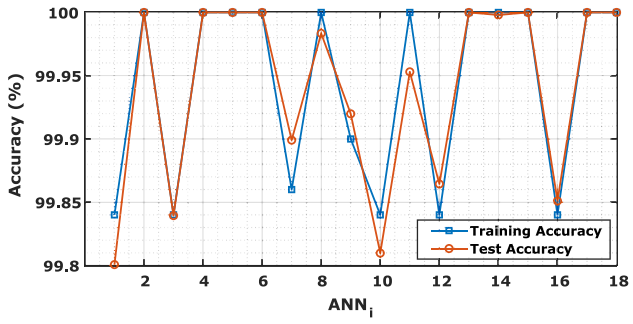


**Fig. 6.** Validation (blue) and test (red) accuracy of each independent network. Total validation accuracy is 98.97 % and total test accuracy is 98.95 %. Total validation accuracy evaluates the probability of all voxels to be correctly predicted.

a good indicator of network performance parameters accuracy. In Fig. 6 a comparison between validation and test accuracy is shown.

In Fig. 7, the number of cases with 0 to 5 errors is shown. This is relevant because the prediction errors can accumulate in a few cases, with several mispredictions in a single case, but they can also be isolated in different cases. Of the total data used for testing, 1140 cases had no mispredicted voxels, while five cases had one misprediction, one case had two mispredictions, and one case had four mispredictions. There are no cases (neither in test nor validation) with more than four mispredictions.

### 3.2. Experimentation results

Experimental evaluation using tissue-mimic gel was performed in 15 cases. Every case was successfully predicted, which means an accuracy of 100 %. This proof of concept shows the viability of this proposal. The experimental evaluation was carried out on 10 corner cases (up to 3 different tumors per case, occupying different voxels, and/or tumors occupying several voxels), and 5 simple cases (tumor touching top or bottom electrodes, in just one or two voxels).

In Fig. 8 one of the experimentation cases is shown. It can be seen that the output of the data processing algorithm matches the real sample. In this presented case, the base agar gel has a conductivity of 0.1 S/m, and the more conductive inserts, 0.2 S/m.

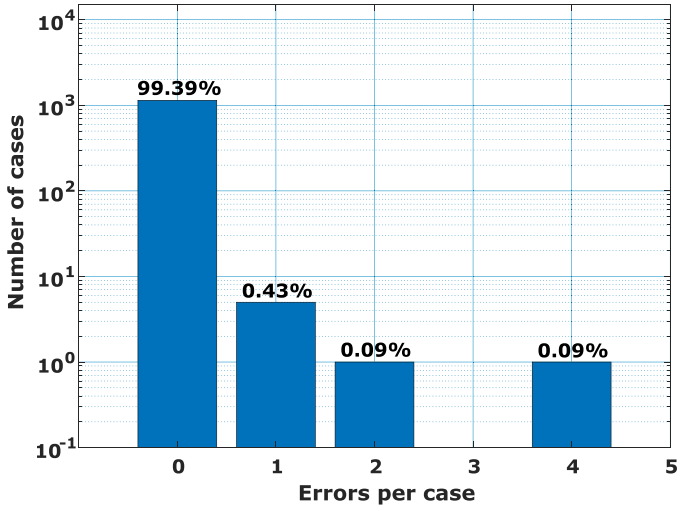


**Fig. 7.** Error Histogram. Number of test cases with 0 to 5 prediction errors. 1140 cases had no mispredicted voxels, while five cases had one misprediction, one case had two mispredictions, and one case had four mispredictions. There are no cases with more than four mispredictions.

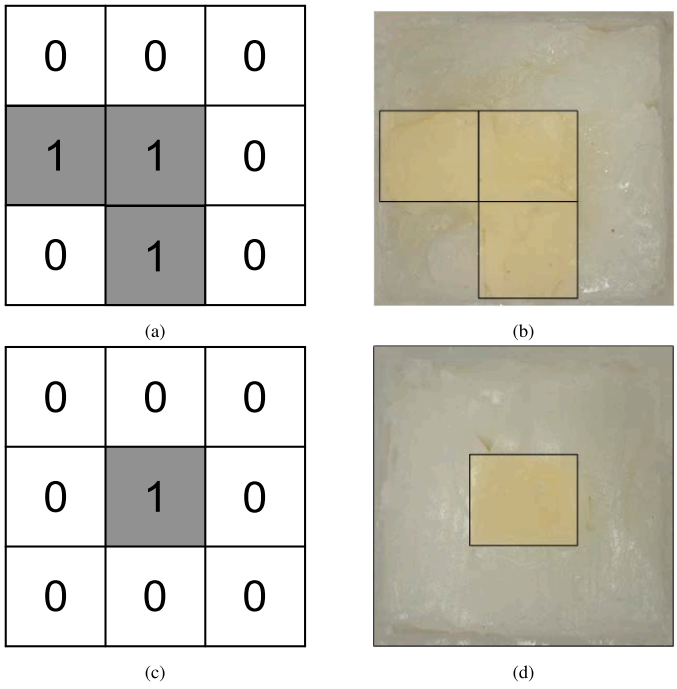


**Fig. 8.** Results. In (a) the estimated top 9 voxels are depicted, while in (c) are shown the bottom one. Those two pictures correspond respectively to (b) and (d), which are the top and bottom face of the same agar sample. The darkened areas are 3 times more conductive than the base gel.

## 4. Discussion and Conclusion

The proposed method allows to locate tumors between the electrodes after placing them. This may allow for a treatment planning that ensures enough electric field on tumor tissue while minimizing healthy tissue damage, thus preventing risks and side effects of the treatment. Although it may not have as much resolution as other methods such as MRI based ones, those cannot be used while electrodes are placed, so it is much more convenient because it is not necessary to relocate or reconnect neither the impedance measurement electrodes, nor the ones for the treatment. This enables a more precise therapy targeting, once the electrodes are placed on the tissue, even if they are not placed with huge precision. It could also allow for a treatment monitoring solution to provide outcome information, but this will need higher network complexity if addressed with machine learning.

Besides, if more precision is needed, more electrodes placed closer to each other, and measuring impedance between the same plate electrodes, would increase it [19]. That said, the precision obtained with this system is enough to ensure a proper electrode placement, plan the treatment, and lately apply it with the same system, targeting the tumors. Moreover, this method could be translated to different multi-electrode setups such as needles, but a finite element model with the new electrodes must be developed. The same method should work as long as the needles have fixed positions.

Although it is not the main of the proposed method, it is able to distinguish between tumor masses spaced at least 10 mm in the plane parallel to the electrode plates, and 2.5 mm in the perpendicular coordinate. It is important to point out that the objective of this method is to find areas with tumor tissue, so it returns the voxels containing at least 5 % of tumor tissue. Considering that every voxel dimensions are $10 \times 10 \times 5$ mm, the minimum tumor volume that can be detected, in the worst-case scenario (tumor exactly between two voxels, with a conductivity of just 2 times the surrounding tissue conductivity), is 50 $mm^3$. This criterion is based on the principle that, although it is important to minimize the effects on healthy tissue, it is essential to ensure that tumor is completely treated. On cases where tumor conductivity is higher, and the tumor mass is all in one voxel, the minimum volume can be as low as 5 $mm^3$. Besides, the treatment-focus capabilities of the hardware are the same as the resolution of this method, so more resolution would not be useful in this scenario.

Partial volume averaging artifacts can be a critical aspect in several imaging methods, such as MRI or EIT. However, the proposed methodology purpose is neither mapping the impedance of the tissue nor the conductivity of each voxel, but only to find where tumor tissue is located based on several impedance measurements. It is also designed to find tumor tissue of only 2 times the healthy tissue conductivity, a lower ratio than usual, in order to detect tumor boundaries easier. So, if there is enough tumor tissue in a voxel to be detected, the algorithm states that the whole voxel contains tumor tissue. This is the criterion followed to train the neural network system, which has been established to avoid leaving untreated tumor tissue. If there is tumor tissue between two adjacent voxels, the algorithm will output that there is tumor tissue in both, and therefore both must be treated.

The proposed algorithm to process data proved to work with the low electrode plates count, where it is not feasible to use the approximations implemented in traditional electrical impedance tomography techniques. Also, the aim of this work is to provide information about where is the tumor tissue and not to provide an impedance tomography map or physiological information like other imaging methods such as MRI. In this sense, if more resolution is desired, the proposed algorithm could be scaled up using a higher electrode and *ANN* count. Moreover, one advantage of single-layered feedforward networks is the low computational cost and speed of calculation, so they can be easily implemented on the control hardware or software of the electroporation voltage generator.

## 5. Funding

This work was partly supported by Projects PID2019-103939RB-I00, PDC2021-120898-I00, TED2021-129274B-I00 and ISCIII PI21/00440, co-funded by MCIN/AEI/10.13039/501100011033 and by EU through FEDER and NextGenerationEU/PRTR programs, and by the DGA-FSE, by Margarita Salas fellowship by the Ministerio de Universidades y la Union Europea - NextGenerationEU, convocatoria de ayudas para la recualificación del sistema universitario español para 2021–2023 and by the DGA under PhD grant.

## Declaration of Competing Interest

The authors declare that they have no known competing financial interests or personal relationships that could have appeared to influence the work reported in this paper.

## Data availability

The authors are unable or have chosen not to specify which data has been used.

## References

[1] E. Luengo, S. Condon, I. Álvarez, J. Raso, Effect of pulsed electric field treatments on permeabilization and extraction of pigments from chlorella vulgaris, J. Membr. Biol. 247 (06 2014). doi:10.1007/s00232-014-9688-2.

[2] M. Sack, C. Eing, T. Berghofe, L. Buth, R. Stangle, W. Frey, H. Bluhm, Electroporation-assisted dewatering as an alternative method for drying plants, IEEE Trans. Plasma Sci. 36 (5) (2008) 2577–2585, https://doi.org/10.1109/TPS.2008.2002440.

[3] G.B. Pintarelli, C.T.S. Ramos, J.R.d. Silva, M.J. Rossi, D.O.H. Suzuki, Sensing of yeast inactivation by electroporation, IEEE Sens. J. 21 (10) (2021) 12027–12035, https://doi.org/10.1109/JSEN.2021.3066092.

[4] Z. Yan, C. Hao, L. Yin, K. Liu, J. Qiu, Simulation of the influence of temperature on the dynamic process of electroporation based on finite element analysis, IEEE Trans. Plasma Sci. 49 (9) (2021) 2839–2850, https://doi.org/10.1109/TPS.2021.3100878.

[5] L.M. Mir, C.Y. Calvet, F.M. Andre, Therapeutic effects of in vivo electroporation: Facilitating drug and gene delivery but not only, in: in: 2014 XXXIth URSI General Assembly and Scientific Symposium (URSI GASS), 2014, pp. 1–3, https://doi.org/10.1109/URSIGASS.2014.6930082.
[6] T. Forjanic, B. Markelc, M. Marcan, E. Bellard, F. Couillaud, M. Golzio, D. Miklavcic, Electroporation-induced stress response and its effect on gene electrotransfer efficacy: In vivo imaging and numerical modeling, IEEE Trans. Biomed. Eng. 66 (9) (2019) 2671–2683, https://doi.org/10.1109/TBME.2019.2894659.
[7] R. Heller, S. Shirley, S. Guo, A. Donate, L. Heller, Electroporation based gene therapy — from the bench to the bedside, Annual International Conference of the IEEE Engineering in Medicine and Biology Society 2011 (2011) 736–738, https://doi.org/10.1109/IEMBS.2011.6090167.
[8] B. Rubinsky, G. Onik, P. Mikus, Irreversible electroporation: A new ablation modality - Clinical implications, Technol. Cancer Res. Treat. 6 (1) (2007) 37–48, https://doi.org/10.1177/153303460700600106.
[9] O. Lucia, H. Sarnago, T. Garcia-Sanchez, L.M. Mir, J.M. Burdio, Industrial electronics for biomedicine: A new cancer treatment using electroporation, IEEE Ind. Electron. Mag. 13 (4) (2019) 6–18, https://doi.org/10.1109/MIE.2019.2942377.
[10] B. Geboers, H. Scheffer, P. Graybill, A. Ruarus, S. Nieuwenhuizen, R. Puijk, M. van den tol, R. Davalos, B. Rubinsky, T. de Gruijl, D. Miklavcic, M. Meijerink, High-voltage electrical pulses in oncology: Irreversible electroporation, electrochemotherapy, gene electrotransfer, electrofusion, and electroimmunotherapy, Radiology 295 (2020) 192190. doi:10.1148/radiol.2020192190.
[11] C. Jiang, R.V. Davalos, J.C. Bischof, A review of basic to clinical studies of irreversible electroporation therapy, IEEE Trans. Biomed. Eng. 62 (1) (2015) 4–20.
[12] E. Maor, A. Ivorra, J. Leor, B. Rubinsky, The effect of irreversible electroporation on blood vessels, Technol. Cancer Res. Treat. 6 (4) (2007) 307–312, https://doi.org/10.1177/153303460700600407.
[13] B. López-Alonso, A. Hernáez, H. Sarnago, A. Naval, A. Guemes, C. Junquera, J. Burdío, T. Castiella, E. Monleón, J. Gracia-Llanes, F. Burdío, E. Mejía, O. Lucia, Histopathological and ultrastructural changes after electroporation in pig liver using parallel-plate electrodes and high-performance generator, Scientific Reports 9 (2019) 2647, https://doi.org/10.1038/s41598-019-39433-6.
[14] M. Faroja, M. Ahmed, L. Appelbaum, E. Ben-David, M. Moussa, J. Sosna, I. Nissenbaum, S.N. Goldberg, Irreversible Electroporation Ablation: Is All the Damage Nonthermal? Radiology 266 (2) (2013) 462–470, https://doi.org/10.1148/radiol.12120609.
[15] R. Davalos, S. Bhonsle, R. Neal, Implications and considerations of thermal effects when applying irreversible electroporation tissue ablation therapy: Ire as a non-thermal therapy, The Prostate 75 (03 2015). doi:10.1002/pros.22986.
[16] Y. Granot, A. Ivorra, E. Maor, B. Rubinsky, In vivo imaging of irreversible electroporation by means of electrical impedance tomography, Phys. Med. Biol. 54 (2009) 4927–4943, https://doi.org/10.1088/0031-9155/54/16/006.
[17] Y. Zhao, H. Liu, S. Bhonsle, Y. Wang, R. Davalos, C. Yao, Ablation outcome of irreversible electroporation on potato monitored by impedance spectrum under multi-electrode system, BioMedical Engineering OnLine 17 (09 2018). doi:10.1186/s12938-018-0562-9.
[18] R. Davalos, D. Otten, L. Mir, B. Rubinsky, Electrical impedance tomography for imaging tissue electroporation, IEEE Trans. Biomed. Eng. 51 (5) (2004) 761–767, https://doi.org/10.1109/TBME.2004.824148.
[19] M. Tang, W. Wang, J. Wheeler, M. McCormick, X. Dong, The number of electrodes and basis functions in eit image reconstruction, Physiol. Meas. 23 (1) (2002) 129, https://doi.org/10.1088/0967-3334/23/1/312.
[20] P. Briz, B. López-Alonso, H. Sarnago, Ó. Lucía, J.M. Burdío, Tumor location method based on multi-electrode structures and machine learning, in: 4th World Congress on Electroporation and Pulsed Electric Fields in Biology, Medicine and Food & Environmental Technologies, International Society for Electroporation Based Technologies and Treatments, 2022.
[21] M. Zappatore, G. Cerfeda, C. Merla, L. Tarricone, Machine learning for h-fire protocols: Tuning parameters for high-frequency irreversible electroporation by machine learning, IEEE Microwave Mag. 22 (2021) 42–59, https://doi.org/10.1109/MMM.2021.3086316.
[22] B. López-Alonso, H. Sarnago, J.M. Burdío, O. Lucía, Multiple output inverter and monitoring system for homogeneous electroporation, IEEE Trans. Power Electron. 38 (2) (2023) 1935–1947, https://doi.org/10.1109/TPEL.2022.3212783.
[23] B. Lopez-Alonso, H. Sarnago, O. Lucia, P. Briz, J.M. Burdio, Real-time impedance monitoring during electroporation processes in vegetal tissue using a high-performance generator, Sensors 20 (3158) (2020), https://doi.org/10.3390/s20113158.
[24] E. Perera-Bel, B. Mercadal, T. García-Sánchez, M.A. González Ballester, A. Ivorra, Modeling methods for treatment planning in overlapping electroporation treatments, IEEE Trans. Biomed. Eng. 69 (4) (2022) 1318–1327. doi:10.1109/TBME.2021.3115029.
[25] T. Rymarczyk, G. Klosowski, E. Kozlowski, A non-destructive system based on electrical tomography and machine learning to analyze the moisture of buildings, Sensors 18 (7) (2018), https://doi.org/10.3390/s18072285.
[26] E. Sontag, Mathematical Control Theory: Deterministic Finite-Dimensional Systems (1998), https://doi.org/10.1007/978-1-4612-0577-7.
[27] D.W. Marquardt, An algorithm for least-squares estimation of nonlinear parameters, J. Soc. Ind. Appl. Math. 11 (2) (1963) 431–441.
[28] B. López-Alonso, H. Sarnago, J.M. Burdío, P. Briz, O. Lucía, Multi-electrode architecture modeling and optimization for homogeneous electroporation of large volumes of tissue, Energies 14 (7) (2021), https://doi.org/10.3390/en14071892.
[29] L.G. Campana, M. Bullo, P.D. Barba, F. Dughiero, M. Forzan, M.E. Mognaschi, P. Sgarbossa, A.L. Tosi, A. Bernardis, E. Sieni, Effect of tissue inhomogeneity in soft tissue sarcomas: From real cases to numerical and experimental models, Technol. Cancer Res. Treatment 17 (2018) 1533033818789693, pMID: 30045667. doi:10.1177/1533033818789693.